Physical Mechanism of Winter Temperature Multidecadal Variations in Arid Central Asia: The Role of the Atlantic Multidecadal Oscillation (AMO)

FEI ZHENG,[a,b] XIAONING LIU,[c] JIANHUI CHEN,[c] WEI HUANG,[c] CHENG SUN,[d] AND HAO WANG[e]

[a] *School of Atmospheric Sciences, Key Laboratory of Tropical Atmosphere-Ocean System, Ministry of Education, Sun Yat-sen University, Zhuhai, China*

[b] *Southern Marine Science and Engineering Guangdong Laboratory, Zhuhai, China*

[c] *Key Laboratory of Western China's Environmental Systems (Ministry of Education), College of Earth and Environmental Sciences, Lanzhou University, Lanzhou, China*

[d] *College of Global Change and Earth System Science (GCESS), Beijing Normal University, Beijing, China*

[e] *Frontiers Science Center for Deep Ocean Multispheres and Earth System, Key Laboratory of Physical Oceanography, Institute for Advanced Ocean Studies, Academy of the Future Ocean, Ocean University of China, Qingdao, China*

(Manuscript received 24 December 2022, in final form 3 May 2023, accepted 3 July 2023)

ABSTRACT: This study investigates the influence of the Atlantic multidecadal oscillation (AMO) on the multidecadal variability of winter surface air temperature in arid central Asia (ACASAT). Apart from a long-term warming trend, the observational analysis shows that the winter ACASAT exhibits a significant multidecadal variability, which is characterized by antiphase fluctuations with the AMO. The mechanism for this negative correlation between the AMO and the winter ACASAT is explored from the aspect of wave teleconnection. The AMO provides energy for the Scandinavian teleconnection pattern at middle and low altitudes by regulating the high-altitude wave train over the middle and high latitudes of Eurasia, and thus has an impact on the remote climate in arid central Asia. Results from the linear baroclinic model (LBM) provide evidence for the linkage between the AMO and the Scandinavian teleconnection pattern. When the AMO is in its warm periods, the Scandinavian teleconnection pattern is in a positive phase, which further makes the cold air from the northeast strengthen, leading to the anomalously colder surface air temperature in arid central Asia. Based on the relationship that the North Atlantic Oscillation (NAO) leads the AMO by 15–20 years, it is further found that there is a leading relationship between the NAO and the winter ACASAT via the AMO. On this basis, an empirical model using the NAO as a predictor was established to predict the ACASAT, and the empirical model shows good hindcast performance. Results from the model show that the winter ACASAT will continue to rise in the next 10 years and decline after 2030.

KEYWORDS: Asia; North Atlantic Ocean; Teleconnections; Climate prediction; Surface temperature; Multidecadal variability

1. Introduction

Global warming has already become an indisputable fact, and the twentieth century saw the fastest rate of warming in nearly a thousand years (IPCC 2013). Studies show that in the cold season, the arid and semiarid regions have exhibited a significant warming trend in the past 100 years (Guan et al. 2019; Huang et al. 2012, 2017a), especially in the middle and high latitudes of the Northern Hemisphere, where the warming amplitude can reach twice the global average land warming amplitude (Huang et al. 2012; Shen et al. 2013; Wang et al. 2008b), accompanied with obvious multidecadal humidity variation characteristics (Huang et al. 2012, 2016). Observations and model simulations taken together suggest that global arid and semiarid regions have continued to expand over the past 60 years, and the expanding rate will accelerate in the twenty-first century (Huang et al. 2017b; Guan et al. 2019).

Arid central Asia (ACA) is a typical inland arid zone, located in the central part of the Eurasian continent. The region has scarce precipitation and sparse vegetation and is the largest nonzoned arid region in the world (Chen et al. 2009, 2011). Due to its special geographical location, ACA is the region of interaction between the westerly climate and the monsoon climate and is sensitive to climate change (Chen et al. 2008, 2010, 2019; Huang et al. 2016; Wang et al. 2008a). Over the past 30–40 years, the warming response of ACA has differed from the total temperature change of Eurasia, with a slow but long-lasting warming rate and consistent warming in the area (Hu et al. 2014; Shen et al. 2013; Sun et al. 2019) (Hu et al. 2014; Shen et al. 2013; Sun et al. 2019). The temperature can be further decomposed into the dynamically induced surface air temperature (SAT), which is influenced by the internal variability of the atmosphere, and the adjusted SAT, which is influenced by the aerosols and greenhouse gases. The dynamically induced SAT shows multidecadal fluctuations, which are different from the continuous increase exhibited by the adjusted SAT (Guan et al. 2015).

Previous studies have pointed out that internal variabilities of SAT in the ACA (ACASAT) are affected not only by local atmospheric influences, but also by remote oceanic and atmospheric factors such as North Atlantic sea surface temperature (SST), Arctic sea ice, European snowpack, and North Pacific SST (Chen et al. 2020a,b; Dai and Deng 2022; Guan et al. 2015, 2019; Li et al. 2022; Mori et al. 2014, 2019; Luo et al. 2019; Zhang et al. 2017). Remote atmospheric factors usually

Corresponding author: Fei Zheng, zhengf35@mail.sysu.edu.cn

DOI: 10.1175/JCLI-D-22-0946.1

cause changes in the climate of the ACA by causing large-scale circulation anomalies; this process can be achieved by exciting or modulating remote atmospheric wave train (Chen et al. 2018, 2020a; Hao et al. 2016; Liu et al. 2022; Sun et al. 2019; Wang et al. 2018). Several studies have suggested that North Atlantic SSTs play an important role in regulating the midlatitude wave train in the Northern Hemisphere and thus affecting the downstream atmosphere (Chen et al. 2018, 2020a; Hao et al. 2016; Li et al. 2015).

As the dominant multidecadal variability signal for North Atlantic SSTs, the AMO plays a role in influencing climate throughout the Northern Hemisphere (Knight et al. 2006). There are several studies showing consistent results about the influence of the AMO on summer ACASAT. In summer, the AMO warm phase promotes precipitation and has a suppressive effect on warming in the ACA (Huang et al. 2015a,b; Hong et al. 2017; Sun et al. 2019; Chen et al. 2023). For winter, the effects of the AMO on the ACASAT are inconsistent among the present literature. For example, using SAT during the period 1957/58–2001, Hao et al. (2016) found that winter ACASAT is positively correlated with the AMO, exhibiting significantly warmer SAT during the positive AMO phase but cooler SAT anomalies in the negative AMO phase. However, using SAT during the period 1950–2015, Luo et al. (2022) found that winter SAT in the ACA is sometimes negatively correlated with the AMO. That is, the effects of the AMO on the ACASAT are inconsistent, and the reason for this inconsistency may be related to the difference in the selection of analyzing period. Considering that the AMO is a multidecadal variability, using SAT data covering a longer period may benefit from identifying its effects on the ACASAT. Therefore, the concentration of this study is the multidecadal relationship between the winter ACASAT and the AMO, using SAT data covering more than 100 years.

In practice, winter SAT is important for the ACA based on the following facts. First, winter temperatures can largely represent the annual mean temperature variations in the ACA and have contributed most to the overall warming slowdown in recent years (Hu et al. 2014; Chen et al. 2023; Shen et al. 2013; Zhang et al. 2016). Second, the widespread warming hiatus in the Northern Hemisphere including the ACA at the beginning of the twenty-first century caused by the AMO and PDO phase shifts, as suggested in previous studies, occurred mainly in winter (Guan et al. 2015, 2017; Luo et al. 2020). Finally, the precipitation in the ACA is dominated by winter and spring. Therefore, clarifying multidecadal winter SAT changes and figuring out the underlying mechanism is important for depicting the overall temperature variability in the ACA and benefits understanding the hydrothermal configuration of this region. In this study, winter denotes December–February.

It is worth noting that there was a 15–20-yr leading relationship between the NAO and the AMO (Seip et al. 2019; Sun et al. 2015). Using reanalysis datasets and numerical simulations, Sun et al. (2015) pointed out that the positive NAO forces the enhancement of the Atlantic meridional overturning circulation (AMOC) and leads to a positive phase of the AMO. The forcing effect is delayed by about 15–20 years, possibly due to the large inertia associated with slow oceanic processes. Based on this leading relationship, empirical models have been established to predict climate up to one or several decades. For example, Li et al. (2013) proposed that the NAO could be used as an effective predictor for Northern Hemisphere mean SAT. The establishment of this empirical model is based on two physical processes: one is the leading relationship between the NAO and the AMO, and the other is the influence of AMO on the Northern Hemisphere mean SAT. Another example is the NAO-based empirical model for East Asian SAT. Similarly, the multidecadal predictability is from the leading relationship between the NAO and the AMO, together with the influence of AMO on East Asian SAT, a linear prediction model is constructed for predicting multidecadal East Asian winter SAT. Considering the 15–20-yr lead–lag relationship between the NAO and the AMO, and supposing the AMO could have impacts on the winter ACASAT, would there exist a leading relationship between the NAO and the winter ACASAT, thus providing multidecadal predictability for the winter ACASAT?

Based on the above questions, the study focuses on whether the AMO can influence the winter ACASAT at multidecadal time scale, and what the specific mechanisms are. Can the NAO provide a source of predictability for multidecadal predictions of winter ACASAT through its modulatory effect on the AMO? Section 2 describes the data and methodology. Section 3 analyzes the impacts of the AMO on the winter ACASAT. Section 4 explores the corresponding mechanisms. Section 5 constructs a physics-based prediction model of the winter ACASAT. Finally, a summary and discussion are given in section 6.

2. Data and methodology

a. *Datasets*

The SAT datasets used in this paper are taken from the global month-by-month surface temperature gridded dataset from the Climatic Research Unit (CRU) at the University of East Anglia for the period January 1901–December 2020. The spatial resolution is 0.5° × 0.5°. The circulation situation data are from the National Oceanic and Atmospheric Administration's (NOAA) Twentieth Century Reanalysis dataset version 3 (20CRv3), and its main advantage is its long time span, covering the global month-by-month grid data from January 1836 to December 2015, with a spatial resolution of 1° × 1°. Of these, data from January 1901 to December 2015 were selected here, including geopotential height, zonal and meridional winds, vertical velocity, air temperature, sensible heat flux, and shortwave and longwave radiation received and emitted by the surface. The HadISST 1.1 monthly average sea surface temperature dataset is used to calculate the AMO-related SST forcing field.

The Atlantic multidecadal oscillation (AMO) is a basin-scale, multidecadal SST anomaly variability that occurs in the North Atlantic region. It is a natural variability with a period of 65–80 years and an amplitude of 0.4°C (Kerr 2000; Li et al. 2009). The North Atlantic Oscillation (NAO) is the most significant mode of the atmosphere in the North Atlantic region and refers to the inverse relationship between the Azores

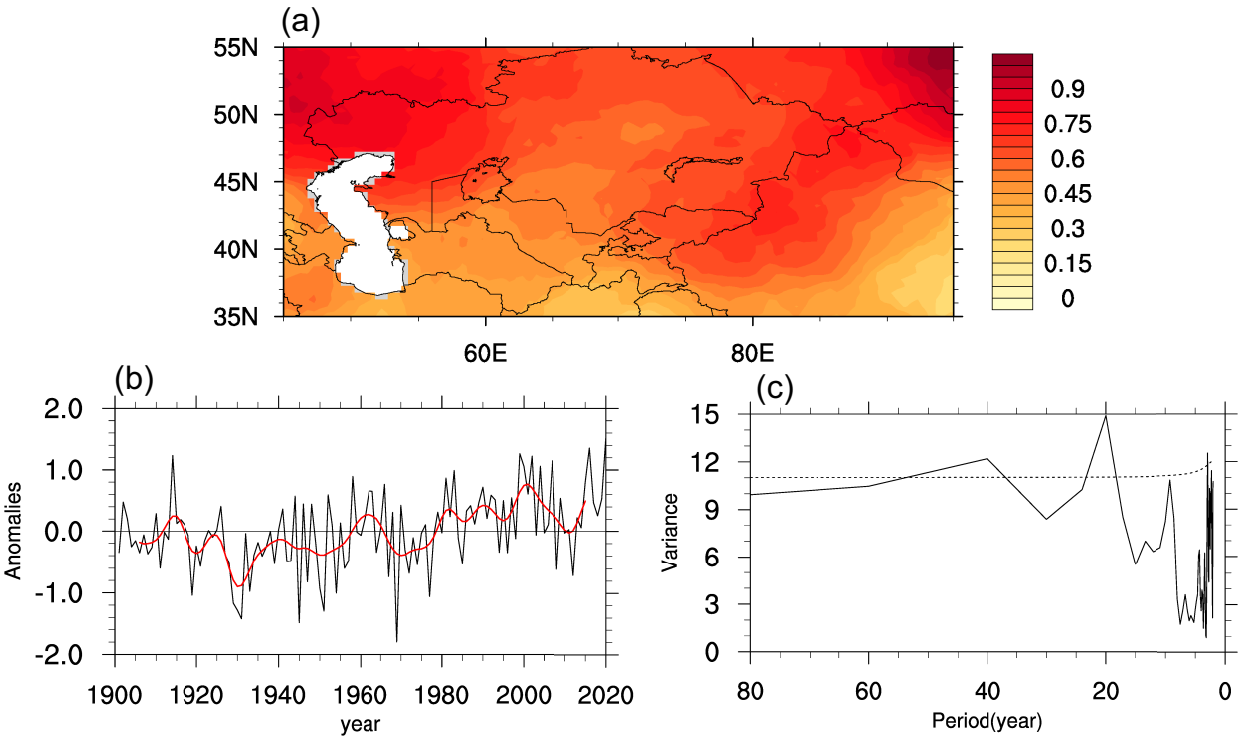

FIG. 1. (a) Warming rate in winter SAT (°C century^{-1}). (b) Time series of regional average winter SAT anomalies in the ACA (°C), hereafter referred to as the ACASAT index; the black line is the original sequence, and the red line denotes the 11-yr low-pass filtered time series. (c) Power spectrum of the ACASAT index; the dashed line is the 95% significance test threshold.

high pressure and Icelandic low pressure (i.e., when the pressure in the Azores is high, the pressure in Iceland is low and vice versa). The NAO and the AMO indices selected for this paper are from the National Centers for Environmental Prediction and National Center for Atmospheric Research (NCEP–NCAR) Climate Data Guide (CDG). The AMO takes the monthly average index, and the NAO is the annual and winter index based on the main component, which is intercepted in this study from January 1901 to December 2020.

The Scandinavian pattern (SCAND) index is for 1950–2020 provided by NOAA's Climate Prediction Center (CPC). However, due to the short time series of this dataset, it is much different from the temperature and circulation situation data. To obtain a longer SCAND index, the REOF decomposition of the 500-hPa geopotential height field in the Northern Hemisphere during winter was performed according to the definition of SCAND by Barnston and Livezey (1987), and region selection is from 20° to 90°N and from 180°E to 180°W. The results of REOF decomposition in spatial distributions are orthogonal to each other and the time series are not orthogonal to each other; the fourth mode represents the SCAND pattern, and its time series is defined as the SCAND index.

b. *Statistical methods*

To obtain multidecadal variation, this study uses the Lanczos low-pass filtering method to filter out the annual signal and retain the multidecadal variation situation for data such as temperature and geopotential height; the filtering window used for low-pass filtering is 11 years to filter out the low-frequency variation. The research focuses on exploring the effect of internal climate variability on surface temperature, so the temperature data are detrended to remove the global warming trend of the last 100 years.

Correlation coefficients and linear regression were used to capture the relationship between two random climate variables, and the significance of the resulting correlation and regression is estimated by the Student's t test. The correlation significance between the circulation situation data and climate index is greatly reduced because of the low-pass filter, Therefore, a more accurate approach is needed for the determination of the test degrees of freedom, which are calculated here according to the method of effective degrees of freedom mentioned in Li et al. (2013).

To replace the original variable field with a smaller number of spatial distribution features and yet cover the signal of the original field, it is necessary to decompose the main spatial distribution pattern of the original field using some mathematical expression. In climate change studies, a common approach is to use empirical orthogonal functions (EOFs) to decompose the original field into linear combinations of orthogonal functions (Lorenz 1956). In this paper, the EOF decomposition is used to identify the main modes of ACASAT variation in winter and the Northern Hemisphere teleconnection wave trains affecting the ACASAT to determine the corresponding situation from high altitude to the ground.

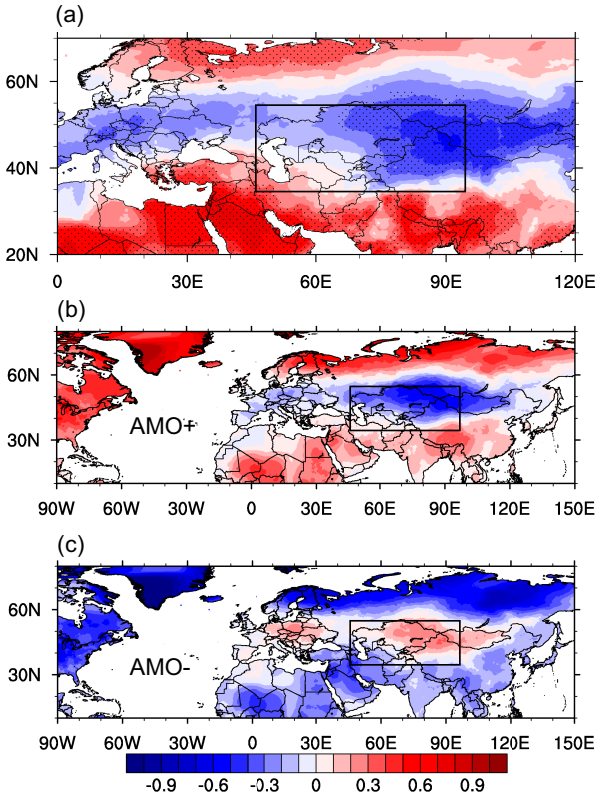

FIG. 2. (a) Correlation between multidecadal winter SAT and the AMO (both low-pass filtered for 11 years). The dotted area represents significant values at the 95% confidence level. Winter SAT anomalies (°C) during the (b) positive and (c) negative phases of the AMO. Positive phases are taken from 1930 to 1960 and 2000 to 2015, and negative phases are taken from 1901 to 1925 and 1970 to 1990. The black box area denotes the area of interest, i.e., the ACA.

c. *Dynamical diagnosis*

The wave action flux is applied to study the energy propagation of Rossby waves. The wave action flux is parallel to the group velocity of net Rossby waves and a useful indicator for identifying the direction and source of constant Rossby wave propagation in the atmosphere (Sun et al. 2017). The wave action fluxes in this paper are calculated according to the method of Takaya and Nakamura (1997, 2001), indicating the propagation of constant Rossby waves associated with a specific teleconnection pattern, independent of the wave phase (Liu et al. 2014).

d. *Model simulation*

In this paper, the linear baroclinic model (LBM) diagnostic experiments were performed to isolate the direct effect of AMO-related diabatic heating. In LBM, diabatic heating and transient momentum flux convergence are treated as forcing, and the direct response of the atmosphere to these forcings is obtained by performing forward integration by the LBM to approximate a steady solution under the background basic flow and appropriate dispersion and diffusion. The basic climate state of the diagnostic experiments is the mean climate state of the winter (December–February) from 1981 to 2000. The SST forcing field is quantified by SST anomalies between the positive and negative AMO phases, and the long-term warming trend in SST are removed before subtracting. The forcing area is 0°–60°N, 7.5°–75°W. In this paper, the last 3-day average of the 30-day integration is selected to express the linear response of atmospheric circulation. The setting of the LBM experiments is described in Sun et al. (2019).

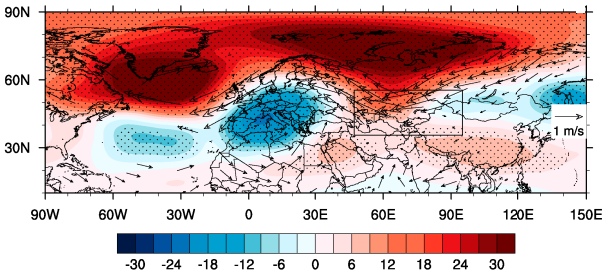

FIG. 3. Regression of winter 500-hPa geopotential height (m) and 850-hPa wind (m s^{-1}) on the AMO index for 1901–2015 (all low-pass filtered for 11 years). The dotted area represents significant values at the 95% confidence level. Only when wind is significant at 95% confidence level, vectors are shown. The black box area denotes the area of interest, i.e., the ACA.

3. Impacts of the AMO on multidecadal winter ACASAT

The core area of the "westerlies-dominated climatic regime" is the main part of the central Asian arid zone (Huang et al. 2015a), which is the main area of interest in this study (i.e., the ACA) (Fig. 1a). To investigate variation in the ACASAT and its corresponding atmospheric circulation anomalies, the first step is to learn about the spatial and temporal distribution of temperature in the ACA. There is overall consistent warming in winter in arid central Asia, with faster warming in western Kazakhstan and near the Pamir Plateau, and relatively slow warming in other regions (Fig. 1a). The average annual warming rate of ACASAT in the past hundred years is 1.9°C $century^{-1}$, and the average winter warming rate is 0.61°C $century^{-1}$. Among them, the temperature from 1901 to 1970 continued to fluctuate steadily in a 20-yr cycle, with no significant warming trend overall, and the warming trend increased after 1970; the magnitude of temperature change was more dramatic (Fig. 1b). Besides, the power spectrum analysis of the winter ACASAT index shows a significant signal of 20- and 40-yr cycles, suggesting that the winter ACASAT has a significant multidecadal cycle feature (Fig. 1c). The seasonal characteristics of the AMO are not obvious, showing an overall more consistent basin temperature trend, and its seasonal signal on the multidecadal scale is less different; therefore, we choose the winter season for the AMO index in the following analysis.

Based on 11 years of low-pass filtering and CRU SAT, the distribution of the detrended correlation between the winter AMO index and winter SAT shows that there are significant

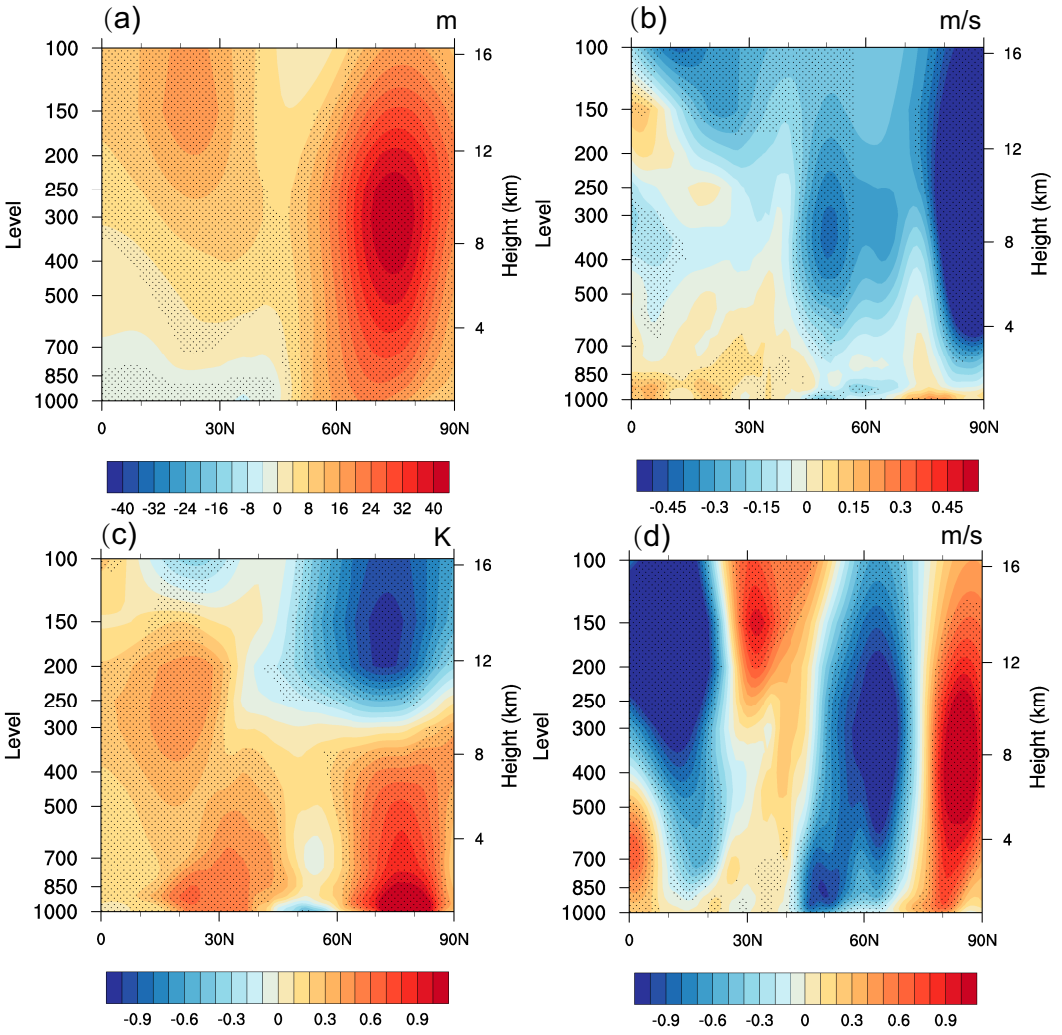

FIG. 4. Regression of zonal mean (45°–95°E) winter (a) geopotential height (m), (b) meridional wind (m s^{-1}), (c) air temperature (K), and (d) zonal wind (m s^{-1}) anomalies on the AMO index for 1901–2015 (all low-pass filtered for 11 years). The dotted areas pass the 95% significance test.

strong negative correlations in eastern central Asia, Xinjiang, and Mongolia (Fig. 2a). The distribution of the negative correlation in the ACA has an east–west distribution difference, with stronger negative correlation in the eastern part and a relatively weaker negative correlation in the western part. To further verify the relationship between the AMO and the winter ACASAT, SAT anomalies during the cold and warm phases of AMO were respectively synthesized, and the results are shown in Figs. 2b and 2c, respectively. The warm phase of AMO was selected from 1930 to 1960 and 2000 to 2015, and the cold phase was from 1901 to 1925 and 1970 to 1990. The central Eurasian region exhibits temperature anomalies different from other regions of the Northern Hemisphere during the AMO warm period, and the negative anomalies of the winter ACASAT are most pronounced (Fig. 2b), whereas during the AMO negative phase period (i.e., when the Atlantic SST is relatively colder) the ACASAT in winter exhibits positive anomalies (Fig. 2c).

The distribution of temperature anomalies during different AMO periods also shows differences between the east and west of arid Central Asia: the temperature anomalies in its eastern part are significantly larger than those in the west during both cold and warm periods of AMO, and the strongest negative correlation is located at the junction of Xinjiang, China, Mongolia, and eastern Kazakhstan. The reason for the above distribution difference is in the circulation anomalies caused by the AMO (Fig. 3). Although there are strong northeasterly wind anomalies in ACA as a whole during the positive phase of the AMO (Fig. 3), which will guide cold air from high latitudes to the region, its western part is located in the southern side of the center of a positive anomaly of geopotential height and there is a sinking movement, and thus the radiative enhancement of warming caused by the sinking movement will offset the cooling due to the northeasterly wind. Meanwhile, its eastern part is located in the western side of the center of a negative anomaly of

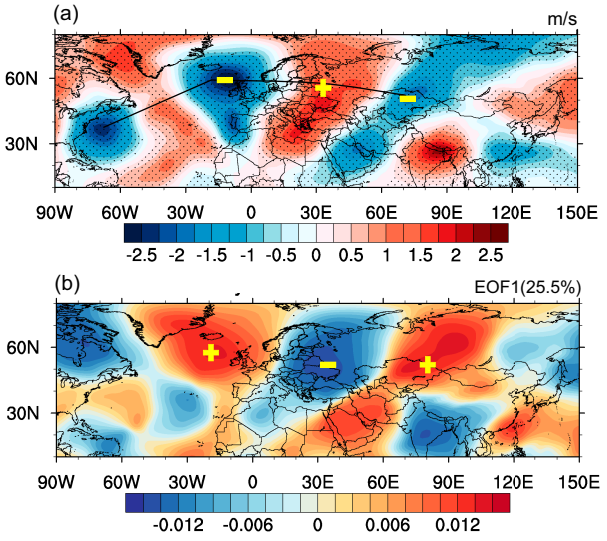

FIG. 5. (a) Regression of 300-hPa meridional wind anomalies (m s^{-1}) on the AMO index. (b) The first mode of EOF decomposition of 300-hPa meridional wind. All are low-pass filtered for 11 years. The dotted areas are those that pass the 95% significance test. The yellow symbols indicate the positive and negative anomaly centers and their locations.

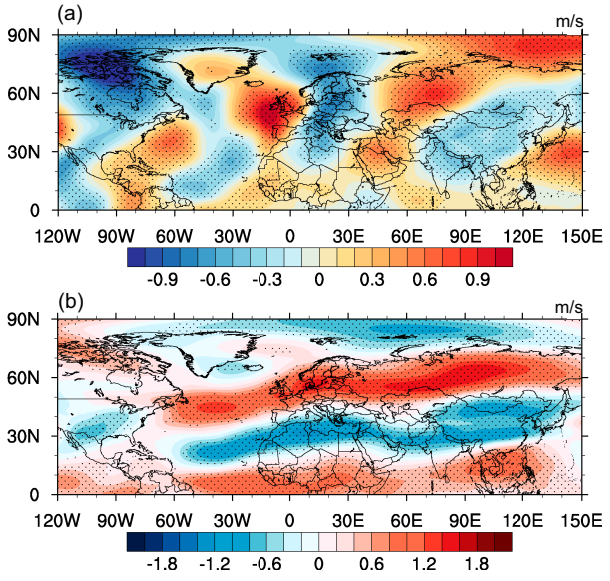

FIG. 6. Regression of winter 300-hPa (a) meridional and (b) zonal wind anomalies (m s^{-1}) on the ACASAT index for 1901–2015. All are low-pass filtered for 11 years. The dotted area passes the 95% significance test.

geopotential height (Fig. 3), and there is an upward movement, which is superimposed with the northeasterly wind, and the cooling situation is enhanced.

4. Dynamical mechanisms of the AMO affecting the winter ACASAT

The above results show that there is a significant negative correlation between the AMO and the winter ACASAT, and the next step is to explore the underlying dynamic mechanism for this remote influence of the AMO. The zonal averages of the geopotential height, air temperature, and zonal and meridional winds in ACA (45°–95°E) were regressed onto the AMO. In the warm period of the AMO, there are positive geopotential height anomalies in high latitudes of the vertical direction, which in turn leads to enhanced surface polar high pressure (Fig. 4a) and the accumulation of cold air on the ground, while the meridional winds near the ground in the middle and high latitudes are negative (Fig. 4b), there are anomalous northerly winds, and the 45°–75°N zonal winds are anomalously negative (Fig. 4d), representing an anomalous easterly component at this point, and the enhanced cold air will flow with the anomalous northeasterly winds near the ground in the middle latitudes to the ACA, which leads to cooling in the middle latitudes, corresponding to negative anomalies in air temperature at the ground (Fig. 4c).

From the regression of AMO and the zonal average of vertical meridional wind anomalies in the midlatitude region of Eurasia (Fig. 4b), there exists a strong anomaly center over 50°N, which is located at 250–300 hPa, whereas it is the zonal average for the whole midlatitude region of the ACA. To further explore whether this anomaly center has a significant influence on the winter ACASAT, we regress meridional wind at 300 hPa onto the AMO index (Fig. 5a). There is a wave train propagating from the central North Atlantic to high latitudes and then southeast to arid Central Asia. As a matter of fact, this wave train is consistent with the first mode of decomposition of 300-hPa meridional wind anomalies (Fig. 5b), and the positions of the anomaly centers correspond to each other with opposite signs. The corresponding time series of the first mode correlates well with the AMO, with a correlation coefficient of −0.54. Since this wave train not only exists on interannual time scale, but also exists on low-frequency multidecadal time scale, we propose the hypothesis that the AMO can influence the atmosphere in remote areas by modulating the wave train.

To confirm that the AMO influences the ACASAT by regulating this remotely related wave train, the wave train can also be obtained by regressing the high-altitude winds from the perspective of ACASAT (Fig. 6a). There are anomalous westerly winds at middle and high latitudes (Fig. 6b), indicating that the high-altitude westerly jet is strengthened, and the center of the anomaly and its overall range correspond well with the wave train, so the latitudinal transmission of the high-altitude train is enhanced, suggesting that the wave train acts as an "atmospheric bridge" between the AMO and the winter ACASAT.

The above study suggests that AMO may affect the winter ACASAT by modulating the high-altitude wave train. Thus, what is the atmospheric circulation process corresponding to the wave train and the change of winter ACASAT? Liu et al. (2014) showed that the North Atlantic Ocean is the energetic origin of several Eurasian teleconnection wave activities in

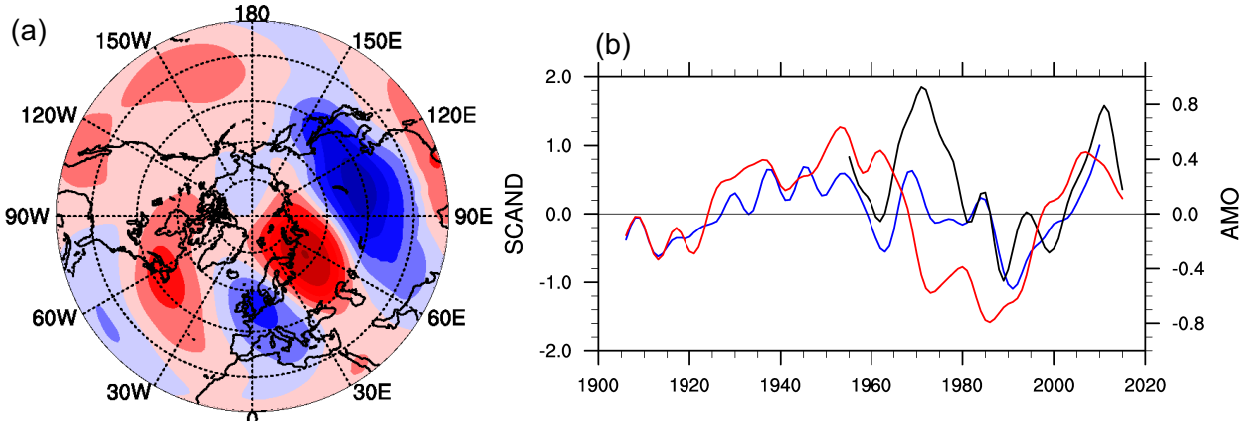

FIG. 7. (a) Spatial distribution of the SCAND pattern, derived from the REOF decomposition of 500-hPa geopotential height field in winter 1901–2015. (b) Temporal evolution of the AMO (red) and the SCAND index derived from the REOF decomposition (blue) and the SCAND index from NOAA (black). All of the three indices have been low-pass filtered for 11 years.

the Northern Hemisphere winter atmospheric modes. Several studies have pointed out that the winter climate in the Eurasian region is related to the Eurasian teleconnection, where the Scandinavian teleconnection (SCAND) is an important mode of regulating surface temperature and precipitation in central Eurasia (Chen et al. 2018; Hao et al. 2016; Liu et al. 2014; Zhuang et al. 2021). The winter SCAND index has multidecadal variability, so one may consider whether the SCAND acts as an intermediate mode connecting the AMO-regulated high-altitude wave train with the ACASAT.

The SCAND pattern is often referred to as the Eurasia-1 pattern (Barnston and Livezey 1987), and its spatial mode is represented by a major atmospheric anomaly center over Scandinavia (Fig. 7a) and a weaker negative center over western Europe and eastern Russia/western Mongolia (Barnston and Livezey 1987; Liu et al. 2014). The SCAND pattern is mainly active in winter and has significant multidecadal characteristics; the spatial mode obtained as in Fig. 7a is by doing the REOF decomposition of the 500-hPa geopotential height field according to the method of Barnston and Livezey (1987). The correlation coefficient between the winter decomposition SCAND index and the SCAND index obtained from NOAA is 0.71 in 1950–2015, significant at the 99% confidence level. Considering the longer time scale of this paper, only results based on the SCAND index obtained by REOF decomposition are shown in the following analysis.

Previous studies have indicated that the SCAND pattern is negatively correlated with the main mode of winter surface temperature in Central Asia at the interannual scale (Zhuang et al. 2021). Previous research on the SCAND teleconnection focused on seasonal and interannual scales, and few have been conducted on multidecadal time scales. Using the SCAND index obtained from the decomposition, it is found that the winter SCAND pattern has multidecadal characteristics (Fig. 7b) and is negatively correlated with the winter ACASAT (figures omitted). The correlation coefficient between the 11-yr low-pass filtered SCAND and ACASAT is −0.64. Meanwhile, the corresponding 500-hPa geopotential height anomalies related to the SCAND pattern are similar to those related to the AMO and the ACASAT (Fig. 8), and the location of

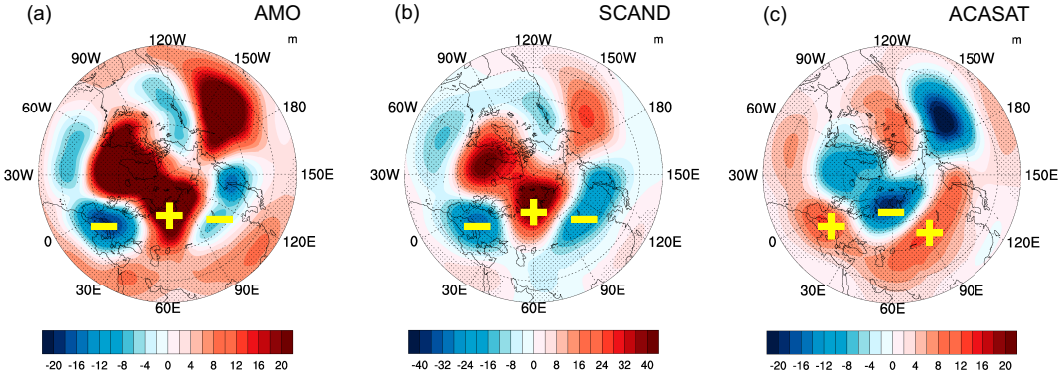

FIG. 8. Regression of winter interdecadal 500-hPa geopotential height (m) on (a) the AMO, (b) the SCAND pattern, and (c) the ACASAT indices. All are low-pass filtered for 11 years. The dotted areas pass the 95% significance test. The yellow symbols indicate the positive and negative anomaly centers and their locations.

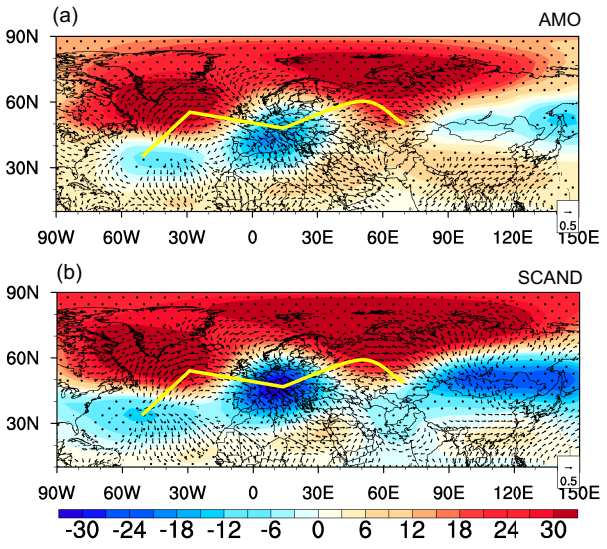

FIG. 9. Regression of 500-hPa geopotential height on (a) the AMO and (b) the SCAND indices (shading; unit: m) and their corresponding T-N wave action fluxes at 200 hPa (arrow indicates direction, and the length indicates magnitude; unit: $m^2\ s^{-2}$). Wind and geopotential height data for wave flux calculation are low-pass filtered for 11 years. The dotted areas pass the 95% significance test. The yellow line is the transmission path of the wave action fluxes.

the anomaly centers in Eurasia is basically the same, with slightly different intensities. The AMO corresponds to the same phase as the SCAND mode, which is opposite to the circulation corresponding to the winter ACASAT.

The SCAND pattern shows a wave train–like structure in the troposphere. The regression of the SCAND index and the 300-hPa meridional wind also corresponds to a wave train (figure omitted), which is similar to the AMO-regulated wave train (Fig. 5b) and the pattern correlation coefficient is −0.82. Meanwhile, the correlation coefficient between the SCAND index and the PC of AMO-regulated wave train is −0.62. To further explain this feature clearly, we calculate the wave action fluxes of the stationary Rossby waves. The Takaya and Nakamura (T-N) wave flux can reflect the energy transmission of Rossby waves aloft (Takaya and Nakamura 1997, 2001). Figure 9 shows that the T-N wave activity fluxes corresponding to the SCAND and the AMO follow almost the same path, both originating from the mid-Atlantic latitudes (20°–50°N, 30°–60°W), conducting northward first, then eastward through southern Greenland to western Europe, and then splitting into two branches, which continue eastward in a wavelike path to arid Central Asia, and the other branch to southeastward to North Africa. According to the transmission path and origin of T-N wave action flux, it is suggested that the SCAND pattern originates in the midlatitudes of the North Atlantic, where the AMO-regulated wave train also originates. The stationary wave energy transmission modulated by the AMO transmits the North Atlantic SST signal through the SCAND pattern to reach arid central Asia, which in turn affects its SAT.

To further explain the specific mechanism of the SCAND pattern affecting the winter ACASAT, we calculate the temperature, wind, and vertical velocity of the vertical direction. The SCAND pattern in its positive phase with negative geopotential height anomaly in the area from northeast China to Mongolia, 90°–120°E (Fig. 9b), with cyclone circulation and anomalous upward motion in the vertical direction (Fig. 10b), while the middle- and low-level temperature over the study region is abnormally low (Fig. 10a), and the upward motion and abnormally cold air make the existence of abnormally cold low pressure in the region and strengthen the East Asian trough at the midlevel, which strengthen the cold air potential at high latitudes, and strong abnormal northeasterly winds from the ground to 60°–120°N at high altitude (Figs. 10c,d). Although there is abnormal sinking motion over arid Central Asia, the warming caused by subsidence is also reflected in the positive temperature anomaly at 400–850 hPa at 60°E in Fig. 10a; meanwhile, the strong northeasterly wind blows the anomalously cold air to the ACA. Therefore, the ACA (45°–90°E) generally shows a cooling situation, but there are differences in the magnitude of cooling from east to west, the reason may be that the cold air from the northeast is stronger in force compared to the possible warming from the sinking motion.

To verify the cooling effect of the AMO on winter ACASAT, we carry out LBM experiments to obtain the direct atmospheric response to the AMO. The SST difference between the warm phase (1935–55) and cold phase (1970–90) of the AMO is used as the forcing field (Fig. 11a), and the forcing area is 0°–60°N, 7.5°–75°W. After the model is stable, the atmospheric response to the AMO shows a negative surface temperature anomaly in the ACA (Fig. 11c), which is consistent with observations. Meanwhile, the corresponding vertical temperature variations (Fig. 11b) is similar to the SCAND pattern (Fig. 10a), which shows a cold anomaly centered at 90°E from the ground to the high altitude. The response of 500-hPa geopotential height also exhibits a mode similar to the SCAND pattern (figure omitted). The LBM experiment results show that the AMO-related warm SST anomalies in the North Atlantic may lead to variations of the SCAND mode and negative air temperature anomalies in the ACA.

In summary, we can conclude that the AMO has a negative correlation with the winter ACASAT on the multidecadal scale, and the underlying mechanism that the AMO provides energy for the SCAND teleconnection at low and medium altitudes by modulating the high-altitude remote connection wave train with a northern position in winter, in turn, has impacts on the remote climate in the ACA. The SCAND pattern is in its positive phase during the AMO warm period, which reduces the net radiation received at the surface of arid Central Asia, and strengthens the cold air from the northeast, resulting in anomalously lower ACASAT.

5. Leading effects of the NAO on winter ACASAT

The mechanism of the AMO affecting the winter ACASAT has been concluded above, it is noteworthy that Li et al. (2013, 2022) proposed that the NAO, as another important climate pattern in the North Atlantic, has a mutual modulation relationship with the AMO. It is found that the NAO leads the AMO by 15–20 years. As the two major climate patterns in the North Atlantic, the NAO and the AMO reflect the variability of air

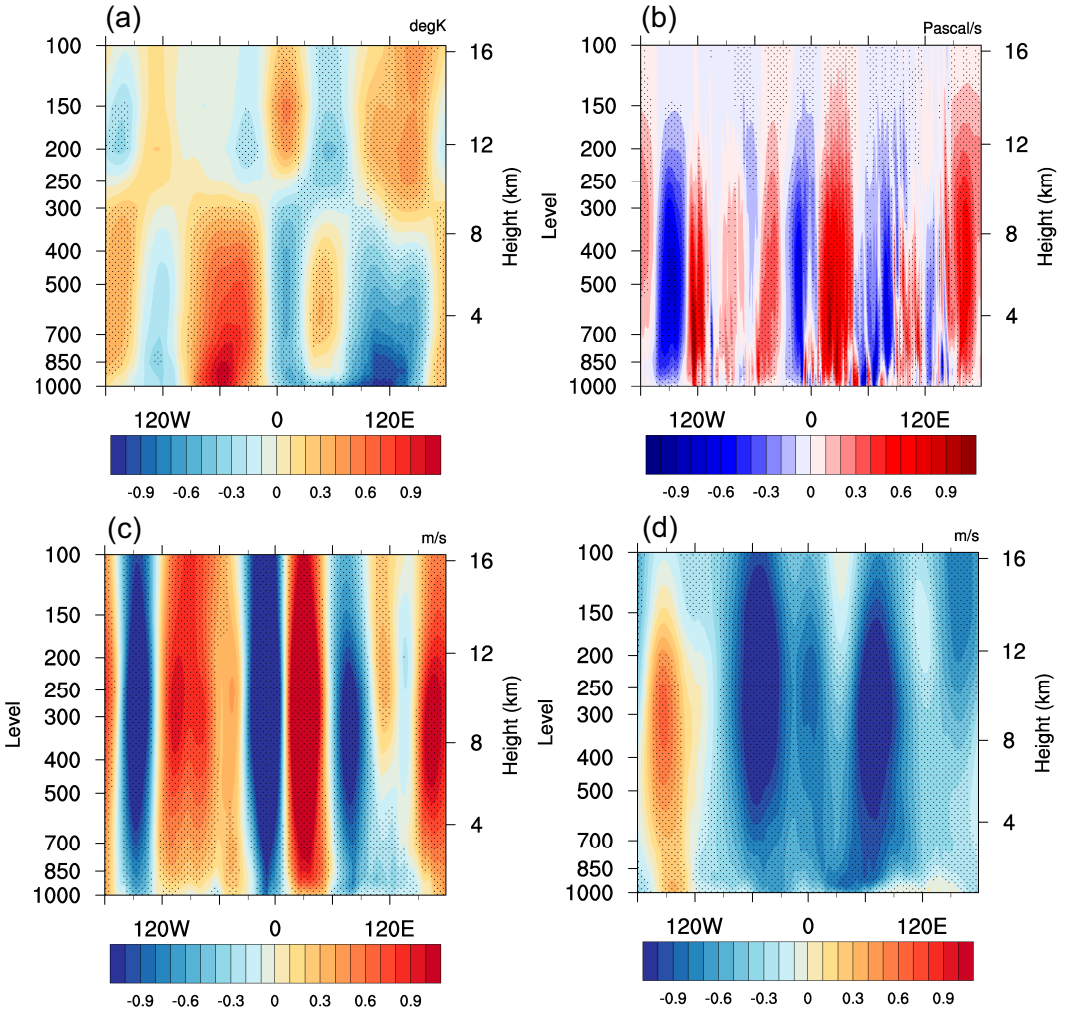

FIG. 10. Regression of winter meridional mean (35°–70°N) (a) air temperature (K), (b) vertical velocity (Pa s^{-1}), (c) meridional wind (m s^{-1}), and (d) zonal wind (m s^{-1}) on winter SCAND index. Vertical velocity is multiplied by −100, and therefore positive and negative values indicate upward and downward motions, respectively. All data are low-pass filtered for 11 years, and dotted areas pass the 95% significance test.

pressure and SST in the North Atlantic. When the NAO is in a positive phase, it will strengthen the positive phase of the North Atlantic tripole SST pattern (NAT), which in turn enhance the Atlantic meridional overturning circulation (AMOC), and the warm seawater at the equator and low latitudes will overturn northward; due to the thermal inertia of SST, this process will delay about 15 years to make the North Atlantic SST increase, which in turn will make the AMO positive phase appear. And then the AMOC continues to strengthen, but due to the slow adjustment of the ocean, the process can last 15–20 years, which in turn makes the SSTs in the midlatitudes of the North Atlantic higher and the negative phase of the NAT, and the negative phase of the NAT leads to the negative phase of the NAO, which in turn makes the AMOC weaken, and the cycle continues (Sun et al. 2015).

Thus, will the leading relationship between the NAO and the AMO affect the winter ACASAT? Assuming there is also a stable leading relationship between the NAO and the winter ACASAT, then whether this relationship can be applied to empirical decadal prediction of the winter ACASAT? It is known that state-of-the-art numerical models usually lack skill for predicting decadal and multidecadal climate variability, because numerical models have a strong dependence on linear responses to anthropogenic forcing and as a result are insufficient for depicting internal multidecadal variations (Meehl et al. 2014; Luo and Li 2014; Xing et al. 2017; Wang et al. 2017). Considering the restriction of numerical models in capturing and predicting multidecadal SAT variability, building a dynamical-based prediction model for multidecadal SAT may benefit the estimation of future temperature variability.

From the multidecadal lead–lag relationship between the NAO index and the winter ACASAT (figure omitted), a strong negative correlation is observed when the NAO leads winter ACASAT by about 20 years. Considering that low-pass filtering

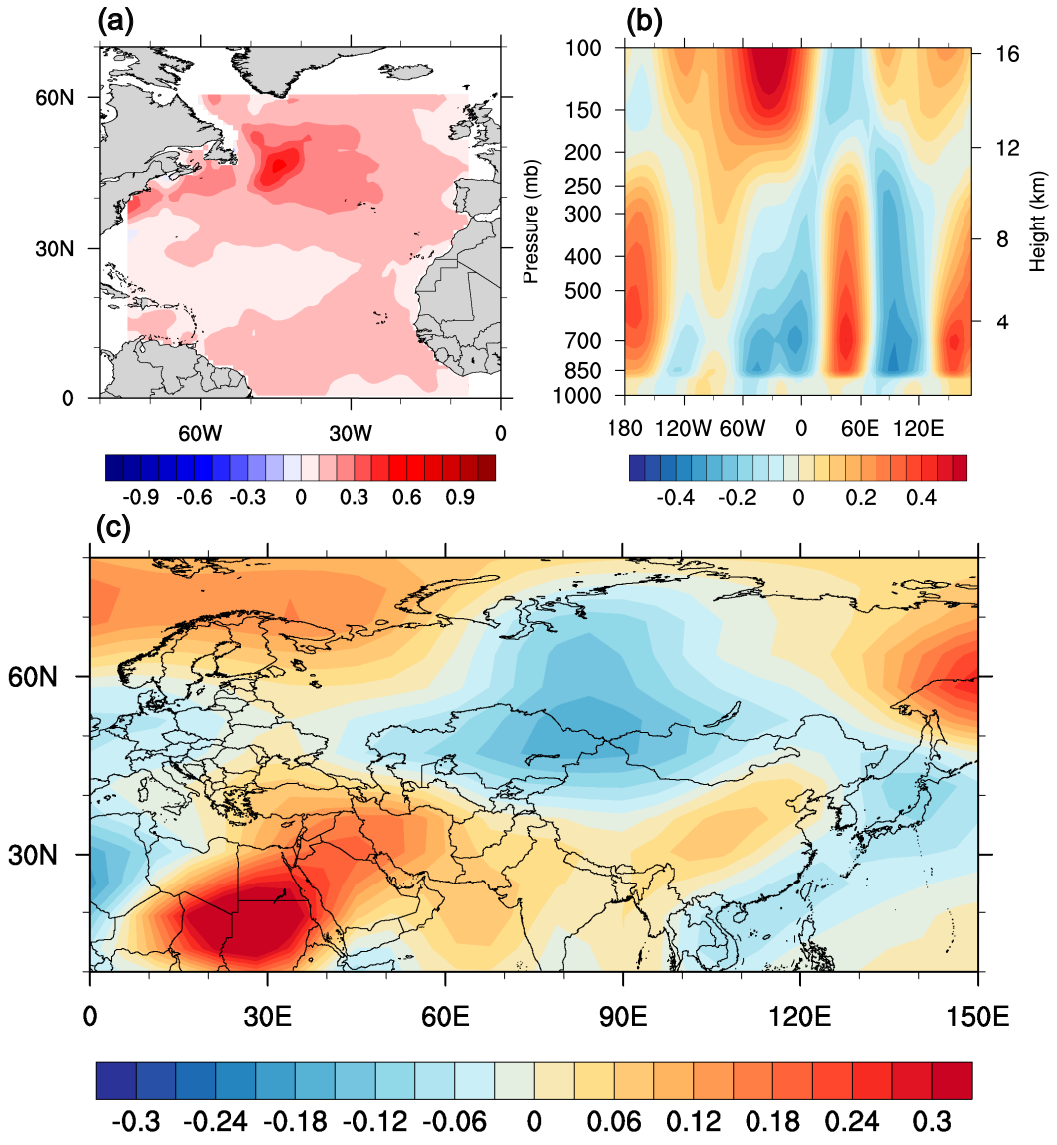

FIG. 11. (a) AMO SST forcing field in the LBM experiment, (b) meridional mean (35°–70°N) of vertical temperature distribution, and (c) land surface temperature response in the LBM experiment.

of the time series will lead to a significant decrease in its effective degrees of freedom, to verify whether the correlation between them is significant, the leading 20-yr correlation between the NAO and winter SAT is calculated and the significance is tested by considering the change in effective degrees of freedom. The results showed that the correlation is still significant between the NAO and winter SAT in most of the arid region of Central Asia (Fig. 12b). Then, this study suggests that the signal of the NAO can be stored in the AMO through 15–20 years and exhibits a negative correlation ahead of the winter ACASAT through the AMO.

As mentioned above, a linear model with the NAO as a predictor is developed for predicting the multidecadal variability of winter ACASAT using a linear regression approach. To remove the effects from the long-term warming trend and consider only the internal atmospheric effects from the NAO, we detrend the NAO and the winter ACASAT, without considering the time term in the model. The prediction model is as follows:

$$\widetilde{T_{\mathrm{dt}}}(t) = a + b \times \mathrm{NAO}_{\mathrm{dt}}(t - 20), \tag{1}$$

where $\widetilde{T_{\mathrm{dt}}}$ is the estimation of the detrended winter ACASAT by the model, t is the time in years, and the coefficients a and b are derived from least squares based on linear regression.

The coefficients a and b in Eq. (1) are −0.29 and −0.71, respectively. To test the performance of the NAO-based multidecadal model, two hindcast experiments were conducted (Figs. 13a,b). In Fig. 13a, only the winter ACASAT from 1926

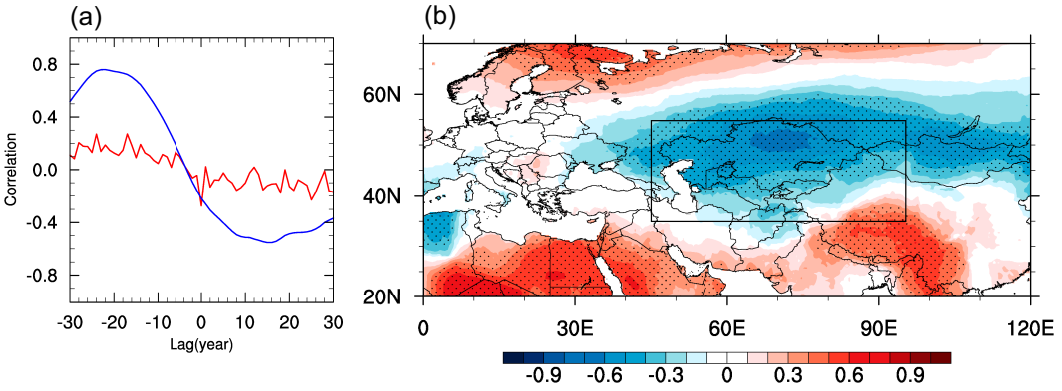

FIG. 12. (a) Lead–lag correlation between annual average AMO and the NAO. The red (blue) line is for the raw (the 11 years low-pass filtering) time series. Negative (positive) lags denote that the AMO lags (leads) the NAO. (b) The lead correlation between the NAO index during 1901–2000 and detrended winter SAT during 1921–2020 based on 11-year low-pass filtering. The dotted area passes the 95% significance test. The black box area denotes the area of interest, i.e., the ACA.

to 1995 was used to estimate model coefficients in Eq. (1), and after the model was built, the ACASAT from 1996 to 2015 was estimated by the model and compared with the observations. A similar hindcast experiment was conducted but the training period is from 1926 to 2000, and the hindcast period is from 2001 to 2015. The forecast interval is quantified by the normal distribution with two standard deviations (the 2-sigma interval). Both experiments capture the time point of multidecadal variation of ACASAT relatively well, but the magnitude of fluctuations is smaller than that of the detrended ACASAT observations. Although the hindcast predictions are overall smaller than the observed values, they have the same trend of temperature change. To match the real future changes of ACASAT more closely in winter, a warming term is added to the model in Eq. (1):

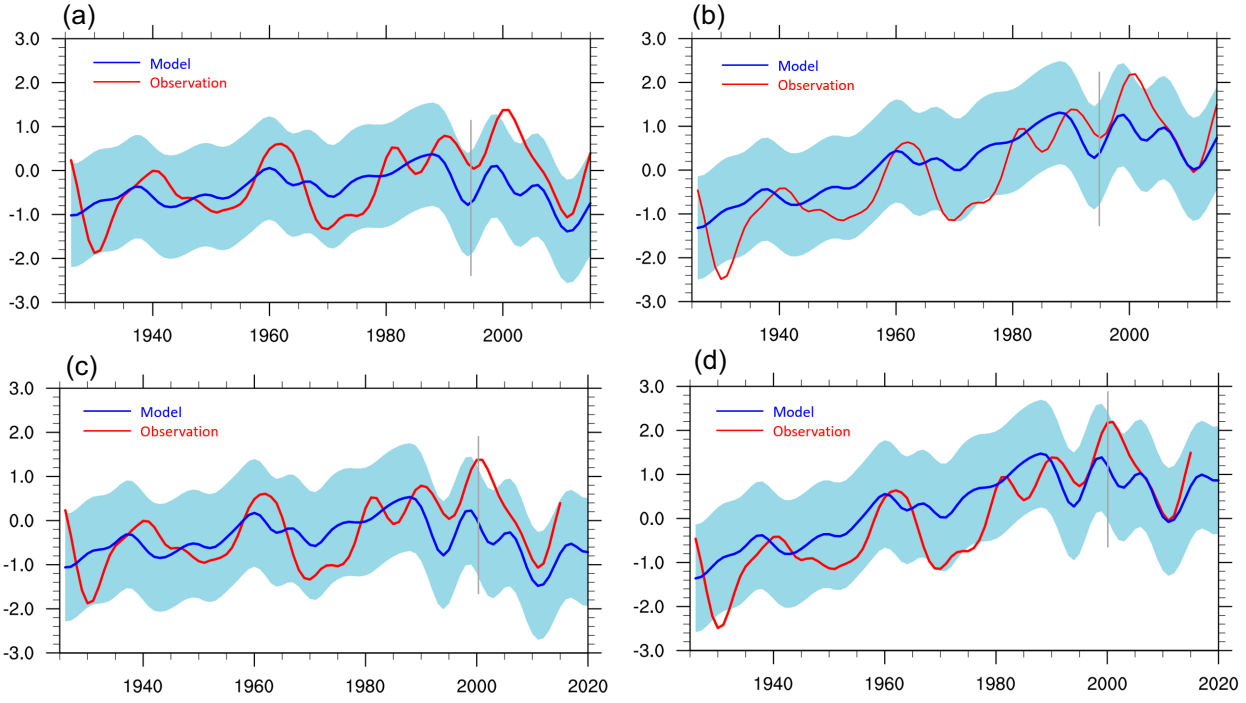

FIG. 13. Observed, simulated, and hindcast winter interdecadal ACASAT (°C). (a) Modeling to predict the winter interdecadal ACASAT from 1995 to 2015 based on detrended winter interdecadal ACASAT from 1925 to 1995 with the NAO from 1905 to 1995, where the red line is observed, the blue line is simulated, and the part behind the gray line is the portion of the hindcast test. (b) As in (a), but for 1925–2000, 1905–2005, and 2000–15. (c) As in (a) but with the addition of the temperature increment term. (d) As in (b), but with the addition of the temperature increment term. The shaded area shows the 2-sigma uncertainty range of the modeled and hindcast values.

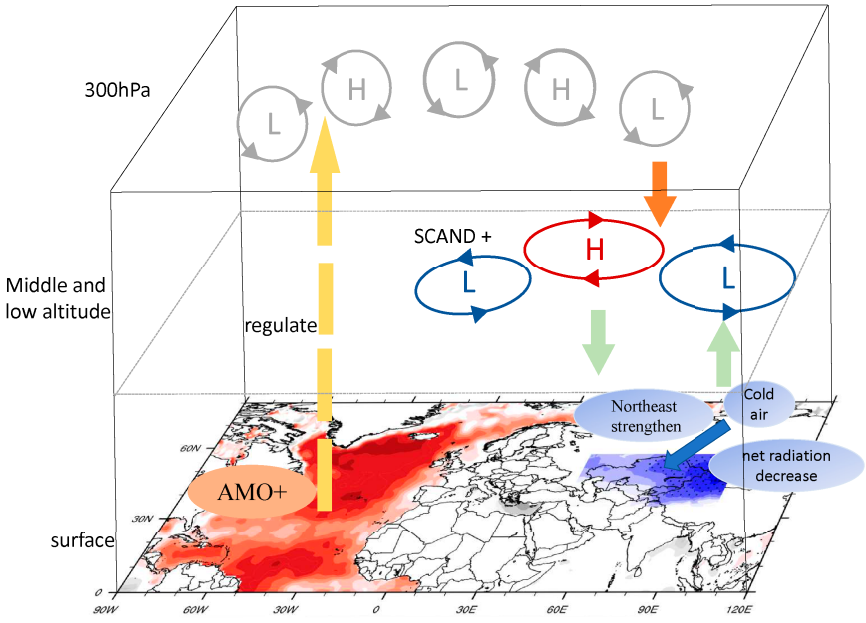

FIG. 14. Schematic diagram illustrating the mechanism of the AMO influence interdecadal winter ACASAT.

$$\tilde{T}(t) = a + b \times \mathrm{NAO}(t - 20) + c \times t, \qquad (2)$$

where c is the average multiyear warming rate.

Then similar hindcast experiments were conducted (Figs. 13c,d). The results show that the prediction model with the addition of the warming term is slightly larger than the observed values in the fitted results before 1990, but the time points of temperature fluctuations in that period still coincide. And for the post-1990 period and the two hindcast predictions, the results are more accurate than the model that does not take into account the warming trend. Thus, the hindcast experiments show that, on the one hand, winter NAO is indeed an effective factor in understanding the multidecadal variability of winter ACASAT, and on the other hand, NAO-based models can be used to make multidecadal predictions of winter ACASAT. It is interesting to note that the prediction performance is better over the period after 1980s, and a possible reason might be related to the stronger link between the NAO and the AMO during this period (figure omitted).

Winter ACASAT for the next 10 years was estimated using the dynamical-based model in Eq. (2). In the decade after 2020, the winter ACASAT will continue to rise until ~2030, with a short, small decline after 2030 (figure omitted).

6. Summary and discussion

In this paper, we investigate the influence of the AMO on winter ACASAT at the modern multidecadal time scale and explore the corresponding mechanism (Fig. 14). Combining the regulatory roles of the NAO on the AMO, we further find a lead–lag relationship between the NAO and the winter ACASAT, then use the NAO as a predictor to predict future multidecadal variations of winter ACASAT. Based on the above work, the following conclusions are drawn.

On a multidecadal time scale, the positive phase of the NAO signal is stored in the ocean, which is reflected in SST changes with a delay of 15–20 years through the interaction between SST and the atmosphere, due to the thermohaline circulation and the thermal inertia of the ocean, making a warm phase of the AMO appear. In winter, the sea surface heats the atmosphere when the AMO is in a warm phase, causing anomalies in the middle- and upper-troposphere circulation, regulating the latitudinal wave train transmitted at middle and high latitudes, providing energy for the transmission of the wave train and the maintenance and activity of the corresponding low-altitude pattern. The wave train connects the North Atlantic Ocean with the remote weather in the middle and high latitudes of Eurasia. While the AMO is in its positive phase, the SCAND mode regulated by SST changes is in its positive phase; at this time there are negative anomalies of geopotential height over arid Central Asia, which makes the net radiation received by the surface decrease, and the anomalous strong northeast wind brings the cold air from high latitudes to arid Central Asia, making the winter ACASAT anomalously low. The AMO cold period has the opposite effect, and the winter ACASAT is abnormally high. Therefore, it is further concluded that when the NAO is in a positive phase, the AMO warm phase will appear after 15–20 years, and then the ACA will have a colder winter, and vice versa. Based on the NAO as a predictor of the temperature variation in the next 20 years, the winter ACASAT will continue to increase in the next decade, and then decrease after 2030.

Combined with previous studies, the wave train regulated by AMO is longstanding, but there may be a north–south shift due to seasonal differences. For example, a similar wave train

was mentioned in the study by Chen et al. (2018, 2020a,b) on spring surface temperature in Eurasia, but its location is slightly different from that of the wave train in this study. The question of whether they are the same wave train needs to be further investigated.

It is worth noting that when decomposing SAT in arid central Asia, the first three modes of winter ACASAT correspond to different Eurasian teleconnection patterns. The SCAND pattern mentioned above corresponds to the main temperature mode with 80% explained variance, the remaining two modes are not discussed separately in this paper due to their smaller explained variance, and the issue of whether the traditional Eurasian teleconnection pattern (EU) and east Atlantic–western Russia pattern (EA–WR) are acting together with the SCAND pattern in ACASAT is open to debate.

The NAO is an important climate mode over the North Atlantic Ocean. Although in this study we only discuss its indirect leading effects on ACASAT via the AMO, its direct effects on the ACASAT on the multidecadal scale cannot be ignored. Several studies have pointed out that the NAO plays an important role in regulating precipitation in the ACA (de Beurs et al. 2018; Guan et al. 2019; Huang et al. 2015a; Liu et al. 2017; Xie et al. 2021; Yang and Zhang 2008; Zhuang et al. 2021). Is there a direct effect of the NAO on air temperature on the multidecadal scale? Or is it possible for the NAO to perturb air temperature by regulating precipitation and then affecting evaporation? All these need to be further explored.

Acknowledgments. Authors Fei Zheng and Xiaoning Liu contributed equally to this work. This work was jointly supported by the National Natural Science Foundation of China (Grants 42371158 and 42375027) and the Natural Science Foundation of Guangdong Province (2023A1515010889). We are thankful to the three anonymous reviewers.

Data availability statement. The global surface temperature dataset used in this study are openly available from the CRU Time Series (TS) version 4.06 of high-resolution gridded data of month-by-month variation at https://catalogue.ceda.ac.uk/uuid/e0b4e1e56c1c4460b796073a31366980. The circulation data are from the 20CRv3 of NOAA (https://psl.noaa.gov/data/gridded/data.20thC_ReanV3.html). The NAO and the AMO indices selected for this paper are openly available from the Climate Data Guide of NCEP/NCAR at https://climatedataguide.ucar.edu/climate-data.The SCAND index is from the NOAA's Climate Prediction Center (CPC) at https://psl.noaa.gov/data/climateindices/list/.

REFERENCES

Barnston, A. G., and R. E. Livezey, 1987: Classification, seasonality and persistence of low-frequency atmospheric circulation patterns. *Mon. Wea. Rev.*, **115**, 1083–1126, https://doi.org/10.1175/1520-0493(1987)115<1083:CSAPOL>2.0.CO;2.

Chen, F. H., and Coauthors, 2008: Holocene moisture evolution in arid central Asia and its out-of-phase relationship with Asian monsoon history. *Quat. Sci. Rev.*, **27**, 351–364, https://doi.org/10.1016/j.quascirev.2007.10.017.

——, J. H. Chen, and W. Huang, 2009: A discussion on the westerly dominated climate model in mid-latitude Asia during the modern interglacial period (in Chinese). *Earth Sci. Front*, **16**, 23–32, https://doi.org/10.3321/j.issn:1005-2321.2009.06.003.

——, and Coauthors, 2010: Moisture changes over the last millennium in arid central Asia: A review, synthesis and comparison with monsoon region. *Quat. Sci. Rev.*, **29**, 1055–1068, https://doi.org/10.1016/j.quascirev.2010.01.005.

——, W. Huang, L. Y. Jin, J. H. Chen, and J. S. Wang, 2011: Spatiotemporal precipitation variations in the arid central Asia in the context of global warming. *Sci. China Earth Sci.*, **54**, 1812–1821, https://doi.org/10.1007/s11430-011-4333-8.

——, and Coauthors, 2019: Westerlies Asia and monsoonal Asia: Spatiotemporal differences in climate change and possible mechanisms on decadal to sub-orbital timescales. *Earth-Sci. Rev.*, **192**, 337–354, https://doi.org/10.1016/j.earscirev.2019.03.005.

Chen, S., R. Wu, L. Song, and W. Chen, 2018: Combined influence of the Arctic Oscillation and the Scandinavia pattern on spring surface air temperature variations over Eurasia. *J. Geophys. Res. Atmos.*, **123**, 9410–9429, https://doi.org/10.1029/2018JD028685.

——, ——, W. Chen, K. Hu, and B. Yu, 2020a: Structure and dynamics of a springtime atmospheric wave train over the North Atlantic and Eurasia. *Climate Dyn.*, **54**, 5111–5126, https://doi.org/10.1007/s00382-020-05274-7.

——, ——, ——, and B. Yu, 2020b: Recent weakening of the linkage between the spring Arctic Oscillation and the following winter El Niño–Southern Oscillation. *Climate Dyn.*, **54**, 53–67, https://doi.org/10.1007/s00382-019-04988-7.

Chen, Z., R. Wu, Y. Zhao, and Z. Wang, 2023: Roles of dynamic and thermodynamic effects in seasonal mean surface air temperature trends over central Asia during 1979–2018. *Climate Dyn.*, **60**, 2331–2342, https://doi.org/10.1007/s00382-022-06457-0.

Dai, A., and J. Deng, 2022: Recent Eurasian winter cooling partly caused by internal multidecadal variability amplified by Arctic sea ice–air interactions. *Climate Dyn.*, **58**, 3261–3277, https://doi.org/10.1007/s00382-021-06095-y.

de Beurs, K. M., G. M. Henebry, B. C. Owsley, and I. N. Sokolik, 2018: Large scale climate oscillation impacts on temperature, precipitation and land surface phenology in central Asia. *Environ. Res. Lett.*, **13**, 065018, https://doi.org/10.1088/1748-9326/aac4d0.

Guan, X., J. Huang, R. Guo, and P. Lin, 2015: The role of dynamically induced variability in the recent warming trend slowdown over the Northern Hemisphere. *Sci. Rep.*, **5**, 12669, https://doi.org/10.1038/srep12669.

——, ——, and ——, 2017: Changes in aridity in response to the global warming hiatus. *J. Meteor. Res.*, **31**, 117–125, https://doi.org/10.1007/s13351-017-6038-1.

——, J. Ma, J. Huang, R. Huang, L. Zhang, and Z. Ma, 2019: Impact of oceans on climate change in drylands. *Sci. China Earth Sci.*, **62**, 891–908, https://doi.org/10.1007/s11430-018-9317-8.

Hao, X., S. He, and H. Wang, 2016: Asymmetry in the response of central Eurasian winter temperature to AMO. *Climate Dyn.*, **47**, 2139–2154, https://doi.org/10.1007/s00382-015-2955-9.

Hong, X., R. Lu, and S. Li, 2017: Amplified summer warming in Europe-West Asia and Northeast Asia after the mid-1990s. *Environ. Res. Lett.*, **12**, 094007, https://doi.org/10.1088/1748-9326/aa7909.

Hu, Z., C. Zhang, Q. Hu, and H. Tian, 2014: Temperature changes in central Asia from 1979 to 2011 based on multiple datasets. *J. Climate*, **27**, 1143–1167, https://doi.org/10.1175/JCLI-D-13-00064.1.

Huang, J., X. Guan, and F. Ji, 2012: Enhanced cold-season warming in semi-arid regions. *Atmos. Chem. Phys.*, **12**, 5391–5398, https://doi.org/10.5194/acp-12-5391-2012.

——, M. Ji, Y. Xie, S. Wang, Y. He, and J. Ran, 2016: Global semi-arid climate change over last 60 years. *Climate Dyn.*, **46**, 1131–1150, https://doi.org/10.1007/s00382-015-2636-8.

——, and Coauthors, 2017a: Dryland climate change: Recent progress and challenges. *Rev. Geophys.*, **55**, 719–778, https://doi.org/10.1002/2016RG000550.

——, H. Yu, A. Dai, Y. Wei, and L. Kang, 2017b: Drylands face potential threat under 2°C global warming target. *Nat. Climate Change*, **7**, 417–422, https://doi.org/10.1038/nclimate3275.

Huang, W., J. H. Chen, X. J. Zhang, S. Feng, and F. H. Chen, 2015a: Definition of the core zone of the "westerlies-dominated climatic regime", and its controlling factors during the instrumental period. *Sci. China Earth Sci.*, **58**, 676–684, https://doi.org/10.1007/s11430-015-5057-y.

——, S. Feng, J. Chen, and F. Chen, 2015b: Physical mechanisms of summer precipitation variations in the Tarim basin in northwestern China. *J. Climate*, **28**, 3579–3591, https://doi.org/10.1175/JCLI-D-14-00395.1.

IPCC, 2013: *Climate Change 2013: The Physical Science Basis*. Cambridge University Press, 1535 pp., https://doi.org/10.1017/CBO9781107415324.

Kerr, R. A., 2000: A North Atlantic climate pacemaker for the centuries. *Science*, **288**, 1984–1985, https://doi.org/10.1126/science.288.5473.1984.

Knight, J. R., C. K. Folland, and A. A. Scaife, 2006: Climate impacts of the Atlantic multidecadal oscillation. *Geophys. Res. Lett.*, **33**, L17706, https://doi.org/10.1029/2006GL026242.

Li, J., C. Sun, and F.-F. Jin, 2013: NAO implicated as a predictor of Northern Hemisphere mean temperature multidecadal variability. *Geophys. Res. Lett.*, **40**, 5497–5502, https://doi.org/10.1002/2013GL057877.

——, T. Xie, X. Tang, H. Wang, C. Sun, J. Feng, F. Zheng, and R. Ding, 2022: Influence of the NAO on wintertime surface air temperature over East Asia: Multidecadal variability and decadal prediction. *Adv. Atmos. Sci.*, **39**, 625–642, https://doi.org/10.1007/s00376-021-1075-1.

Li, S. L., Y. Wang, and Y. Gao, 2009: A review of the researches on the Atlantic multidecadal oscillation (AMO) and its climate influence. *Trans. Atmos. Sci.*, **32**, 458–465, https://doi.org/10.3969/j.issn.1674-7097.2009.03.014.

Li, X., E. P. Gerber, D. M. Holland, and C. Yoo, 2015: A Rossby wave bridge from the tropical Atlantic to West Antarctica. *J. Climate*, **28**, 2256–2273, https://doi.org/10.1175/JCLI-D-14-00450.1.

Liu, H., X. Liu, and B. Dong, 2017: Intraseasonal variability of winter precipitation over central Asia and the western Tibetan Plateau from 1979 to 2013 and its relationship with the North Atlantic Oscillation. *Dyn. Atmos. Oceans*, **79**, 31–42, https://doi.org/10.1016/j.dynatmoce.2017.07.001.

Liu, Y., L. Wang, W. Zhou, and W. Chen, 2014: Three Eurasian teleconnection patterns: Spatial structures, temporal variability, and associated winter climate anomalies. *Climate Dyn.*, **42**, 2817–2839, https://doi.org/10.1007/s00382-014-2163-z.

——, C. Sun, Z. Gong, J. Li, and Z. Shi, 2022: Multidecadal see-saw in cold wave frequency between central Eurasia and Greenland and its relation to the Atlantic multidecadal oscillation. *Climate Dyn.*, **58**, 1403–1418, https://doi.org/10.1007/s00382-021-05967-7.

Lorenz, E., 1956: Empirical orthogonal function and statistical weather prediction. Scientific Rep. No. 1 Statistical Forecasting Project, 52 pp., http://bobweigel.net/csi763/images/pdf/Lorenz1956.pdf.

Luo, B., L. Wu, D. Luo, A. Dai, and I. Simmonds, 2019: The winter midlatitude-Arctic interaction: Effects of North Atlantic SST and high-latitude blocking on Arctic sea ice and Eurasian cooling. *Climate Dyn.*, **52**, 2981–3004, https://doi.org/10.1007/s00382-018-4301-5.

——, D. Luo, A. Dai, I. Simmonds, and L. Wu, 2022: The modulation of interdecadal Pacific Oscillation and Atlantic multidecadal oscillation on winter Eurasian cold anomaly via the Ural blocking change. *Climate Dyn.*, **59**, 127–150, https://doi.org/10.1007/s00382-021-06119-7.

Luo, F. F., and S. L. Li, 2014: Joint statistical-dynamical approach to decadal prediction of East Asian surface air temperature. *Sci. China Earth Sci.*, **57**, 3062–3072, https://doi.org/10.1007/s11430-014-4984-3.

Luo, W., X. D. Guan, Y. L. He, R. Guo, Z. Li, and C. Cao, 2020: Characteristics of temperature variation in warm season over the Northern Hemisphere during the global warming hiatus. *Plateau Meteor.*, **39**, 673–682, https://doi.org/10.7522/j.issn.1000-0534.2019.00031.

Meehl, G. A., H. Teng, and J. M. Arblaster, 2014: Climate model simulations of the observed early-2000s hiatus of global warming. *Nat. Climate Change*, **4**, 898–902, https://doi.org/10.1038/nclimate2357.

Mori, M., M. Watanabe, H. Shiogama, J. Inoue, and M. Kimoto, 2014: Robust Arctic sea-ice influence on the frequent Eurasian cold winters in past decades. *Nat. Geosci.*, **7**, 869–873, https://doi.org/10.1038/ngeo2277.

——, Y. Kosaka, M. Watanabe, H. Nakamura, and M. Kimoto, 2019: A reconciled estimate of the influence of Arctic sea-ice loss on recent Eurasian cooling. *Nat. Climate Change*, **9**, 123–129, https://doi.org/10.1038/s41558-018-0379-3.

Seip, K. L., Ø. Grøn, and H. Wang, 2019: The North Atlantic oscillations: Cycle times for the NAO, the AMO and the AMOC. *Climate*, **7**, 43, https://doi.org/10.3390/cli7030043.

Shen, W. F., Q. Miao, T. Wei, and C. Kong, 2013: Analysis of temperature variation in recent 130 years in central Asia (in Chinese). *J. Arid Meteor.*, **31**, 32–36, https://doi.org/10.11755/j.issn.1006-7639(2013)-01-0032.

Sun, C., J. Li, and F.-F. Jin, 2015: A delayed oscillator model for the quasi-periodic multidecadal variability of the NAO. *Climate Dyn.*, **45**, 2083–2099, https://doi.org/10.1007/s00382-014-2459-z.

——, ——, R. Ding, and Z. Jin, 2017: Cold season Africa–Asia multidecadal teleconnection pattern and its relation to the Atlantic multidecadal variability. *Climate Dyn.*, **48**, 3903–3918, https://doi.org/10.1007/s00382-016-3309-y.

Sun, X., S. Li, X. Hong, and R. Lu, 2019: Simulated influence of the Atlantic multidecadal oscillation on summer Eurasian nonuniform warming since the mid-1990s. *Adv. Atmos. Sci.*, **36**, 811–822, https://doi.org/10.1007/s00376-019-8169-z.

Takaya, K., and H. Nakamura, 1997: A formulation of a wave-activity flux for stationary Rossby waves on a zonally varying basic flow. *Geophys. Res. Lett.*, **24**, 2985–2988, https://doi.org/10.1029/97GL03094.

——, and ——, 2001: A formulation of a phase-independent wave-activity flux for stationary and migratory quasigeostrophic eddies on a zonally varying basic flow. *J. Atmos. Sci.*, **58**, 608–627, https://doi.org/10.1175/1520-0469(2001)058<0608:AFOAPI>2.0.CO;2.

Wang, J. S., F. H. Chen, L. Y. Jin, and F. Wei, 2008a: The response to two global warming periods in the 20th century

over the arid central Asia (in Chinese). *J. Glaciol. Geocryol.*, **30**, 224–233, https://doi.org/10.7522/j.issn.1000-0240.2008.0033.

——, ——, and Q. Zhang, 2008b: Temperature variations in arid and semi-arid areas in middle part of Asia during the last 100 years. *Plateau Meteor.*, **27**, 1035–1045.

Wang, L., G. Huang, W. Chen, W. Zhou, and W. Wang, 2018: Wet-to-dry shift over southwest China in 1994 tied to the warming of tropical warm pool. *Climate Dyn.*, **51**, 3111–3123, https://doi.org/10.1007/s00382-018-4068-8.

Wang, X., J. Li, C. Sun, and T. Liu, 2017: NAO and its relationship with the Northern Hemisphere mean surface temperature in CMIP5 simulations. *J. Geophys. Res. Atmos.*, **122**, 4202–4227, https://doi.org/10.1002/2016JD025979.

Xie, T., W. Huang, S. Chang, F. Zheng, J. Chen, J. Chen, and F. Chen, 2021: Moisture sources of extreme precipitation events in arid central Asia and their relationship with atmospheric circulation. *Int. J. Climatol.*, **41**, E271–E282, https://doi.org/10.1002/joc.6683.

Xing, N., J. Li, and L. Wang, 2017: Multidecadal trends in large-scale annual mean SATa based on CMIP5 historical simulations and future projections. *Engineering*, **3**, 136–143, https://doi.org/10.1016/J.ENG.2016.04.011.

Yang, L., and Q. Zhang, 2008: Effects of the North Atlantic Oscillation on the summer rainfall anomalies in Xinjiang. *Chin. J. Atmos. Sci.*, **32**, 1187–1196, https://doi.org/10.3878/j.issn.1006-9895.2008.05.16.

Zhang, R., R. Zhang, and Z. Zuo, 2017: Impact of Eurasian spring snow decrement on East Asian summer precipitation. *J. Climate*, **30**, 3421–3437, https://doi.org/10.1175/JCLI-D-16-0214.1.

Zhang, Y., J. Xu, Z. Chen, Y. Xu, and L. Bai, 2016: Spatial and temporal variation of temperature in central Asia. *J. Arid Land Resour. Environ.*, **30**, 133–137, https://doi.org/10.13448/j.cnki.jalre.2016.228.

Zhuang, Y., J. Zhang, and L. Wu, 2021: Linkages of surface air temperature variations over central Asia with large-scale climate patterns. *Theor. Appl. Climatol.*, **145**, 197–214, https://doi.org/10.1007/s00704-021-03626-9.